Solar Energy Vol. 44, No. 5, pp. 271–289, 1990
Printed in the U.S.A.

0038–092X/90 $3.00 + .00

MODELING DAYLIGHT AVAILABILITY AND IRRADIANCE COMPONENTS FROM DIRECT AND GLOBAL IRRADIANCE

RICHARD PEREZ, PIERRE INEICHEN, ROBERT SEALS,
JOSEPH MICHALSKY, and RONALD STEWART
Atmospheric Sciences Research Center, State University of New York at Albany,
Albany, NY 12205, U.S.A.

Abstract—This paper presents the latest versions of several models developed by the authors to predict short time-step solar energy and daylight availability quantities needed by energy system modelers or building designers. The modeled quantities are global, direct and diffuse daylight illuminance, diffuse irradiance and illuminance impinging on tilted surfaces of arbitrary orientation, sky zenith luminance and sky luminance angular distribution. All models are original except for the last one which is extrapolated from current standards. All models share a common operating structure and a common set of input data: Hourly (or higher frequency) direct (or diffuse) and global irradiance plus surface dew point temperature. Key experimental observations leading to model development are briefly reviewed. Comprehensive validation results are presented. Model accuracy, assessed in terms of root-mean-square and mean bias errors, is analyzed both as a function of insolation conditions and site climatic environment.

1. INTRODUCTION

Specific solar, HVAC, or daylighting applications require specific solar radiation components for simulation or monitoring purposes. For instance, the simulation of daylight distribution in complex interior spaces, which is now possible thanks to new software development (e.g., [1]), requires an accurate knowledge of the distribution of light in the sky. Because these specific components are many and are often too expensive to measure on a routine basis, one has to rely on conversion models that use more routinely accessible data.

We present in this paper a series of extensively validated models that can generate a comprehensive set of such components and contribute to bridging the gap between available solar radiation data and specific user needs. Model applications are manyfold. Two examples are (i) the preparation of local climatological data bases for direct use by interested engineering parties—this is currently being done for several locations in the State of New York [2]—and (ii) the modification of the radiation processing algorithms of specific system simulation programs (e.g., [3]). The models are the result of a three year development/validation study performed on experimental data recorded at 10 American and three European sites. Climates and environments range from high altitude desert to temperate maritime, including humid continental, subtropical and highly polluted environments.

Although the models' end-use fields may be very different, their common input and structure calls for this single unifying paper. This may contribute to presenting solar resource assessment as a global question rather than a combination of research fields which have all too often evolved on parallel tracks in the past.

2. METHODS

2.1 *Model overview*

The models presented in this paper are of three types;

1. Luminous efficacy models that relate, in terms of number of lumens per watt, the three basic radiation components—direct, global and diffuse irradiance—to their photopic equivalent—direct, global, and diffuse illuminance. Illuminance may be defined as the yield of a given light source—in the present case, the sun/sky—when its spectrum is weighted by the transfer function of the human eye [4]. The International Illumination Commission (CIE) standard human eye response curve and solar spectrum are compared in Fig. 1.
2. Models that predict diffuse irradiance or illuminance received by tilted surfaces.
3. Models that are concerned with the angular distribution of light in the sky dome rather than with the integrated diffuse values as in (2). A model that predicts the luminance at the sky's zenith is proposed and evaluated along with a model, extrapolated from CIE standards [5]–[7], that estimates luminance at any point in the sky dome.

All models are "all-weather" short-time-step conversion algorithms with a common operating structure. They are validated here with both hourly and 15-minute data.

The interrelationship between models, input data and main application fields may be seen in Fig. 2.

2.2 *Modeling approach*

2.2.1 *Model input and insolation condition parameterization.* The input to the models consist of short-time-step (hourly or less) direct and global ir-

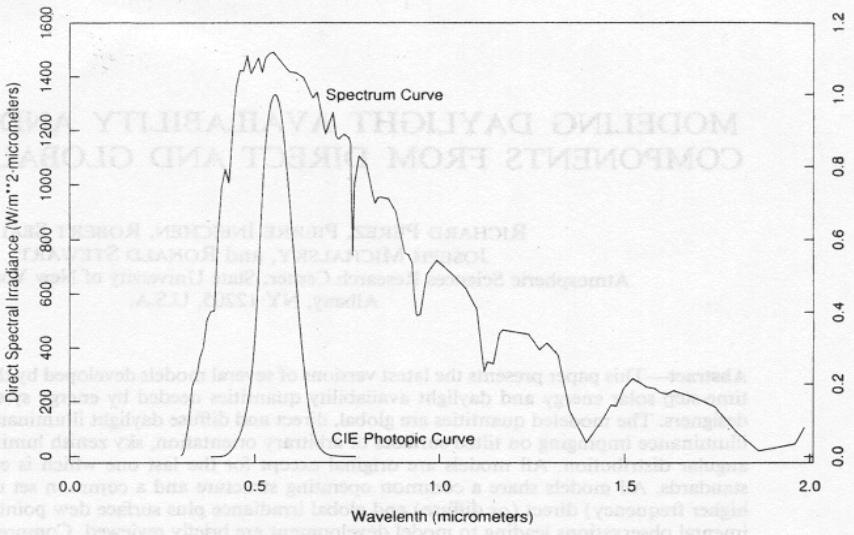

Fig. 1. The CIE Human Eye Photopic curve plotted with respect to the solar spectrum.

radiance data, as well as, for those where spectral effects are of concern, three-hourly surface dew point temperature. Global and direct irradiance constitute today the most widely available type of solar radiation data. Moreover, the recent development of the low cost/maintenance rotating shadowband radiometer suggest that these will be more widely available in the future networks[8,9]. Modeled input may be used, in the absence of either the direct or both quantities, with a corresponding loss in accuracy[10]. The other input

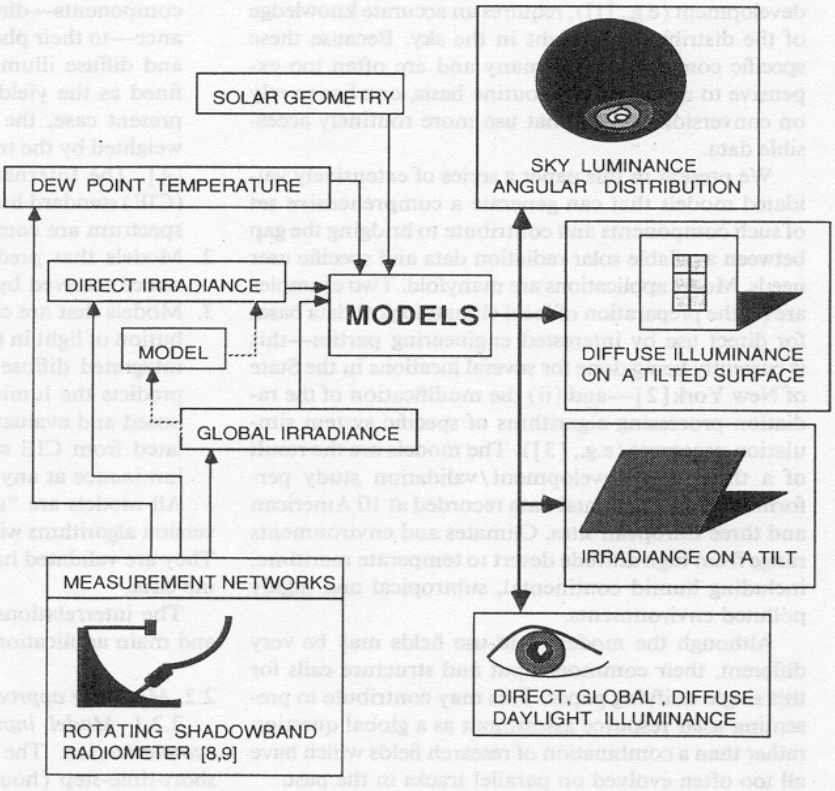

Fig. 2. Interrelationship between model inputs and outputs. The models' input data may be readily supplied by the Rotating Shadowband Radiometer, a new instrument well suited for precise network operation[9].

to some of the models presented here, 3-hourly surface dew point temperature is a widely available standard met orological parameter.

The above inputs are processed to derive four basic components that parameterize all insolation conditions from overcast to clear. These components are

(1) The solar zenith angle, noted as Z;

(2) The sky's clearness, noted as ϵ and given by

$$\epsilon = [(Dh + I)/Dh + \kappa Z^3]/[1 + \kappa Z^3], \quad (1)$$

where Dh is the horizontal diffuse irradiance, I the normal incidence direct irradiance and κ a constant equal to 1.041 for Z in radians; the Z^3 formulation was added to the original, simpler ϵ expression to eliminate dependence between this component and the solar zenith angle.

(3) The sky's brightness, noted as Δ and given by

$$\Delta = Dh * m/I_o, \quad (2)$$

where m is the relative optical airmass[11] and I_o the extraterrestrial irradiance.

(4) The atmospheric precipitable water content, denoted W(cm), and given by

$$W = \exp(0.07 * Td - 0.075) \quad (3)$$

where Td (°C) is the three-hourly surface dew point temperature.

The formulation in eqn (3) is similar to that proposed by Reitan[12] which is applicable to monthly averages and validated for 15 locations in the United States. Its validity for short-time-step data was experimentally validated in the context of this project by Wright *et al.*[13].

It will be noted that the Δ-ϵ parameterization used here carries a quantity of information equivalent to the *K-kt* or *kd-kt* representations often reported in the literature[14,15]. However, it is thought that the present approach better separates two distinct characteristics of the atmosphere: (i) ϵ variations express the transition from a totally overcast sky to a low turbidity clear sky; (ii) Δ variations reflect the opacity/thickness of the clouds.

2.2.2 *Models structure.* All the models presented here have a common structure represented by the following equation:

$$Y = X * F(\text{insolation condition, receptor/sun geometry}) \quad (4)$$

where Y is the modeled quantity (e.g., zenith luminance), X is a quantity depending only on the three basic inputs specified above, (e.g., diffuse irradiance), and F is a transfer function depending on the insolation condition components and solar geometry. The function F combines an analytical formulation for the variables Δ, Z and W and a discrete (bin) formulation for the variable ϵ. This semianalytical formulation allows for maximum computer calculation efficiency—discrete data table access is much less time consuming than computations—while allowing manageable hand calculations if necessary (see discussion in [16]). In most instances, the dependence of F on insolation conditions will be expressed as

$$F(\epsilon,\Delta,Z,W) = a_i(\epsilon) + b_i(\epsilon)f(W) + c_i(\epsilon)g(Z) + d_i(\epsilon)h(\Delta) \quad (5)$$

where f, g, and h are analytical functions and a_i, b_i, c_i and d_i are discrete functions represented by eight-term vectors corresponding to eight ϵ bins. These bins have been optimized to account for the observed variability of sky radiance distribution at several site[17] are specified in Table 1.

2.2.3 *Model derivation.* All models presented and tested here, with the exception of the luminance angular distribution model, were experimentally derived. The terms of the function F specified above were obtained in each case through least-square fitting of large data sets representative of a variety of climatic environments. Note that the structure of the function F is not entirely statistical but reflects in many cases the physical properties of radiation transfer.

2.3 *Experimental data*

Experimental data from a total of 13 sites are used in this study for model derivation and/or model validation purposes[42–46]. These are listed in Table 2 along with their dominant climatic/environment characteristics, the length of the available data set and the frequency of experimental measurements.

A typical instrumentation set-up used for 10 out of 13 sites[17,20] is shown in Fig. 3. Table 3 identifies measurements available at each site and indicates if data from the site were used in this study for model derivation purposes or strictly for independent validation purposes. Note that both 15-minute and hourly data where used indiscriminately in this paper for model derivation and validation purposes, hence the "short-time-step" term used to qualify the models.

Data are known in each case to be of high quality and to have undergone strict calibration monitoring and stringent quality control. Class I pyrano/pyrheliometers were used in all cases except for the vertical irradiance measurements in the New York locations. The cosine responses of each pyranometer and photometer used for the derivation of luminous efficacy

Table 1. Discrete sky clearness categories

ϵ category	lower bound	upper bound
1. Overcast	1	1.065
2.	1.065	1.230
3.	1.230	1.500
4.	1.500	1.950
5.	1.950	2.800
6.	2.800	4.500
7.	4.500	6.200
8. Clear	6.200	--

Table 2. Origin, size and climatic environment of experimental data sets

Site	Climate/Environment Main Features	Data Set Span and Frequency
Geneva, Switzerland [42]	Temperate maritime, with central Europe continental influence. Persistent nebulosity enhanced by "blocking position at foot-hill of the Alps.	1 yr. hourly data
Trappes, France [43]	Temperate maritime with high incidence of intermediate skies	3 yr. hourly data
Carpentras, France [43]	Mediterranean	3 yr. hourly data
Albany, NY, USA [44,45]	Humid continental with bimodal	3yr. hourly data 2 yr. 15 min. data
New York, NY, USA [45]	Humid continental with maritime influence plus large City's anthropogenic environment	1 yr. 15 min. data
Farmingdale, NY, USA [45]	Same as above but without city's environment	1 yr. 15 min. data
Oswego, NY, USA [45]	Humid continental, Great Lakes basin	6 mo. 15 min. data
Glens Falls, NY, USA [45]	Humid continental	6 mo. 15 min. data
Phoenix, AZ, USA [46]	Arid, low elevation	6 mo. hourly data
Albuquerque, NM, USA [46]	Arid, High elevation (1800 m)	1 yr. hourly data
Los Angeles, CA, USA [46]	Arid and maritime influence plus high frequency of anthropogenic smog events	6 mo. hourly data
Osage, KS, USA [46]	Continental, U.S. Great Plains	6 mo. hourly data
C. Canaveral, FL, USA [46]	Subtropical, low latitude, maritime	6 mo. hourly data

models were experimentally determined. Data were corrected to account for this source of error, which may become critical at low elevations, particularly if the illuminance and irradiance sensors have opposite responses, as was often the case. This process is reported and thoroughly discussed in [18,19].

3. RESULTS

Result presentation is structured as follows: for each model, a brief review of experimental observations is first presented, followed by the formulation of the model and validation results.

3.1 *Luminous efficacy models*

Much observational work and modeling has occurred over the last 50 years to estimate luminous efficacy for specific insolation conditions and locations (e.g., see the comprehensive review by [21] and recent work by [22,23]). However, until very recently, no model development effort was undertaken to systematically predict the three photopic component from their irradiance equivalent for all insolation conditions. The following luminous efficacy models were derived from over 25,000 data points in five northeast U.S. locations [20]. They are validated against data from each of these sites plus, independently, against data from one European site using similar instrumentation [24].

3.1.1 *Global irradiance to illuminance conversion.*

Key Observations. Experimental values of global luminous efficacy, G_{eff}, as a function of several sky condition parameters have been plotted in Fig. 4. These include (i) variations of G_{eff} with sky clearness ϵ for $Z \sim$ constant; (ii) variations with sky brightness Δ for overcast conditions and $\sim$ constant Z; (iii) variations with zenith angle for very clear ($\epsilon > 6$) and, (iv) "average" ($0.1 < \Delta < 0.3$) overcast conditions ($\epsilon < 1.2$). A polynomial fit to data, illustrating the combined variations of Geff with Δ and ϵ, may be found in Fig. 5. The two previous figures include all data available from Geneva, and the five New York State sites.

Features previously noted by the authors [25] are quite apparent through these plots. Of particular interest is the exponential variation of G_{eff} with brightness, observed for overcast conditions. This has also been noted since by Littlefair [26]. This is attributable to the increase of water vapor absorption, hence the increase in luminous efficacy, with cloud thickness. One

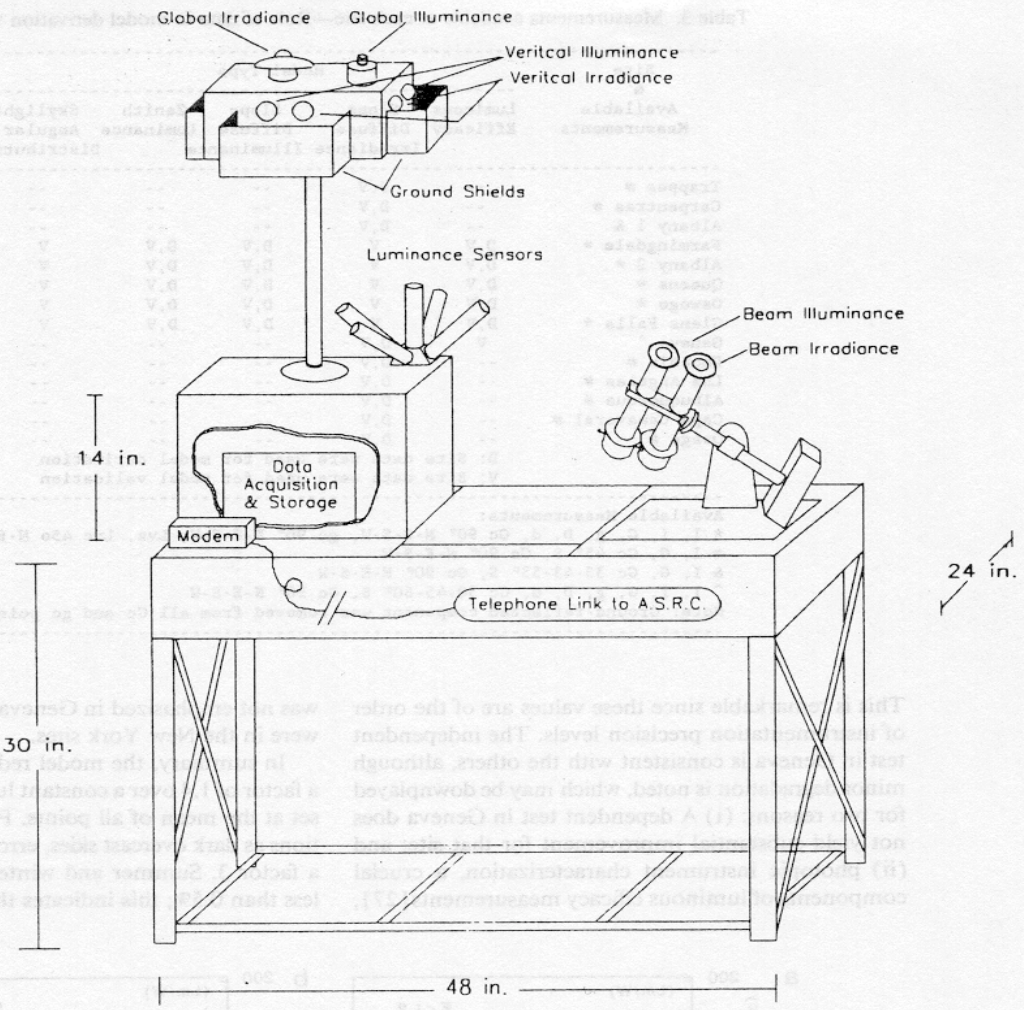

Fig. 3. Typical data acquisition set-up.

will also note from Fig. 4 that the clear sky zenith angle effect is minimal but that a noticeable zenith angle trend is observed for overcast conditions. A more detailed presentation and discussion of these results may be found in [20].

Of importance is the fact that observations independently performed in five distinctive northeastern U.S. and one Swiss location are in good agreement, suggesting that model site dependency may not be a major obstacle. This statement is supported by Fig. 6 where G_{eff} variations with Δ for the 50°–70° zenith angle range are compared for each of the six sites.

Model formulation. Equation (6) below is used to calculate global illuminance from irradiance and the sky condition parameters. This was derived from 25,000 data points from the five New York State sites:

$$g = G[a_i + b_i W + c_i \cos(Z) + d_i \, Ln(\Delta)] \quad (6)$$

The coefficients a_i, b_i, c_i, and d_i are given in Table 4 for each ϵ bin.

Model validation. Performance evaluation results are summarized in Table 5. This includes model RMSE and MBE for three ranges of insolation conditions (respectively, overcast, intermediate, and clear) and six locations. The Geneva test is independent, the five other tests are technically dependent, since the test data were used to derive the model. However note that, for this and the other models tested here, a set of environmentally distinct sites are considered over a wide seasonal range. The testing process considers each site/season/insolation conditions distinctly; a satisfactory behavior of the model for each element in this comprehensive range of environments may be considered as a valid testing ground, especially if one realizes that quality independent data sets of this type are particularly scarce today. Of course, subsequent independent testing is strongly recommended; the CIE's International Daylighting Measurement Year Program [41] should provide the data needed for these verifications.

Resultant RMSE for all six sites is 3% while MBE is kept near or below 1% for all conditions and sites.

Table 3. Measurements available at each site—Role of data in model derivation validation

Site & Available Measurements	Model Type: Luminous Efficacy	Slope Diffuse Irradiance	Slope Diffuse Illuminance	Zenith Luminance	Skylight Angular Distribution
Trappes #	--	D,V	--	--	--
Carpentras #	--	D,V	--	--	--
Albany 1 &	--	D,V	--	--	--
Farmingdale *	D,V	V	D,V	D,V	V
Albany 2 *	D,V	V	D,V	D,V	V
Queens *	D,V	V	D,V	D,V	V
Oswego *	D,V	V	D,V	D,V	V
Glens Falls *	D,V	V	D,V	D,V	V
Geneva ^	V	D,V	--	--	--
Phoenix #	--	D,V	--	--	--
Los Angeles #	--	D,V	--	--	--
Albuquerque #	--	D,V	--	--	--
Cape Canaveral #	--	D,V	--	--	--
Osage #	--	D,V	--	--	--

D: Site data were used for model derivation
V: Site data were used for model validation

Available Measurements:
* I, i, G, g, D, d, Gc 90° N-E-S-W, gc 90° N-E-S-W, Lvz, Lvc 45o N-E-S-W
# I, G, Gc 45° S, Gc 90° N-E-S-W
& I, G, Gc 33-43-53° S, Gc 90° N-E-S-W
^ I, i, G, g, D, d, Gc 30-45-60° S, Gc 90° N-E-S-W
Note: Ground-reflected component was removed from all Gc and gc points

This is remarkable since these values are of the order of instrumentation precision levels. The independent test in Geneva is consistent with the others, although minor degradation is noted, which may be downplayed for two reasons: (i) A dependent test in Geneva does not yield substantial improvement for that site; and (ii) photopic instrument characterization, a crucial components of luminous efficacy measurements [27], was not emphasized in Geneva to the extent that they were in the New York sites.

In summary, the model reduces overall RMSE by a factor of 1.4 over a constant luminous efficacy model set at the mean of all points. For such specific conditions as dark overcast skies, error reduction approaches a factor 3. Summer and winter bias are found to be less than 0.5%; this indicates that the model accounts

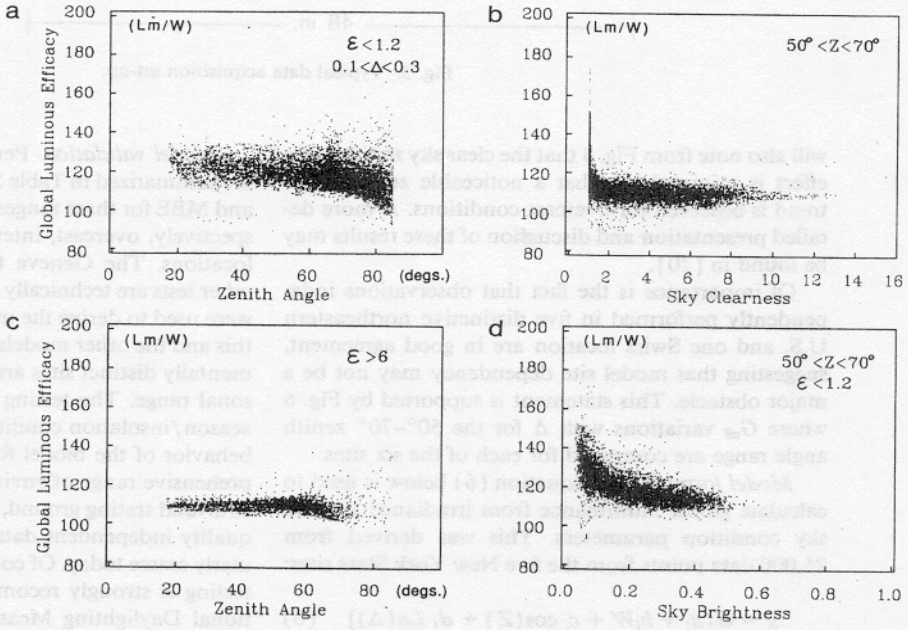

Fig. 4. Variations of global luminous efficacy with (a) Solar zenith angle for overcast conditions. (b) Sky Clearness, ϵ, for a limited zenith angle range. (c) Solar zenith angle for very clear conditions. (d) Sky Brightness, Δ, for overcast conditions. (Data from five New York sites and Geneva).

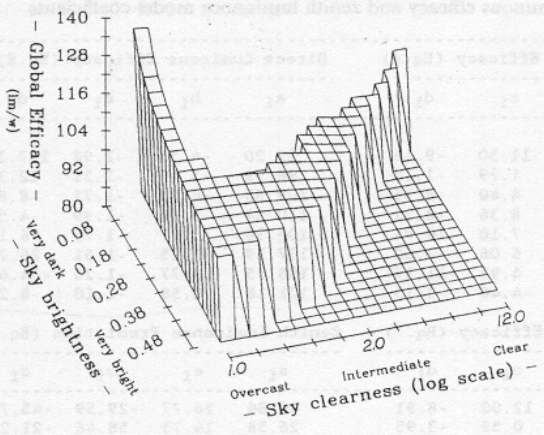

Fig. 5. Best-fit polynomial surface showing combined variations of global luminous efficacy with ϵ and Δ at Z and Td = constant. (Note that the surface is plotted only for the ϵ-Δ plane region where the quasi-totality of events were recorded—the remaining of the plane corresponds to either extremely unlikely (low Δ, middle ϵ) or to physically impossible situations (high Δ, high ϵ).

satisfactorily for seasonal differences that have been previously reported [28].

3.1.2 *Diffuse irradiance to illuminance conversion.*

Key Observations. Variations of diffuse luminous efficacy, D_{eff}, with ϵ have been plotted in Fig. 7 for each of the six sites. A similar trend is apparent at each site showing a marked increase from overcast to clear conditions caused by an increased contribution of molecular (Rayleigh) scattering. (Note that the values of ϵ (sky clearness) achieved in Geneva ware far below those achieved at the New York sites; this is a result of climatic differences reported in Table 2). A polynomial surface has been fitted to the ensemble of data (Fig. 8) to illustrate the combined variations of D_{eff} with clearness and brightness at $Z \sim$ cst. This varies from less than 110 lumen/watt for bright overcast conditions to above 150 for clear skies. Clear sky luminous efficacy further increases with solar zenith angle, likely because of increased contribution, on the horizontal, of multiple Rayleigh scattering at the expense of circumsolar Mie scattering; this may be seen in Fig. 9. As before, a more detailed analysis of results will be found in [20].

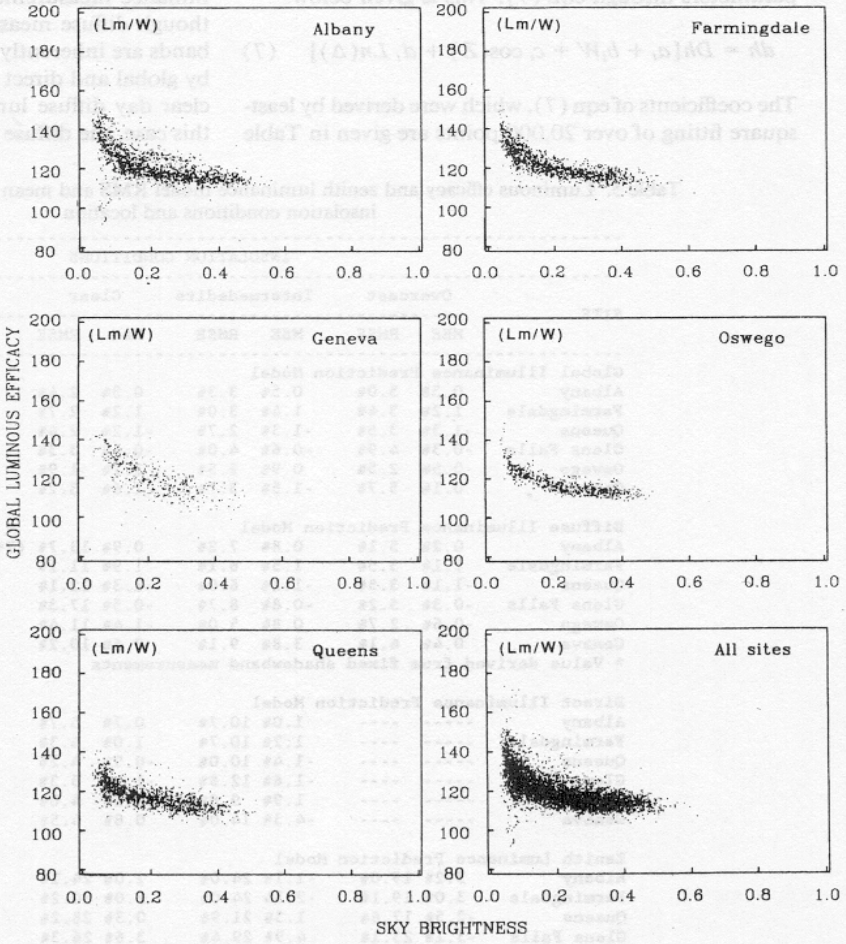

Fig. 6. Variations of global luminous efficacy with sky brightness, Δ, for five locations.

Table 4. Luminous efficacy and zenith luminance model coefficients

	Global luminous Efficacy (Eq.6)				Direct Luminous Efficacy (Eq.8)			
ϵ bin	a_i	b_i	c_i	d_i	a_i	b_i	c_i	d_i
1	96.63	-0.47	11.50	-9.16	57.20	-4.55	-2.98	117.12
2	107.54	0.79	1.79	-1.19	98.99	-3.46	-1.21	12.38
3	98.73	0.70	4.40	-6.95	109.83	-4.90	-1.71	-8.81
4	92.72	0.56	8.36	-8.31	110.34	-5.84	-1.99	-4.56
5	86.73	0.98	7.10	-10.94	106.36	-3.97	-1.75	-6.16
6	88.34	1.39	6.06	-7.60	107.19	-1.25	-1.51	-26.73
7	78.63	1.47	4.93	-11.37	105.75	0.77	-1.26	-34.44
8	99.65	1.86	-4.46	-3.15	101.18	1.58	-1.10	-8.29

	Diffuse Luminous Efficacy (Eq.7)				Zenith Luminance Prediction (Eq.10)			
ϵ bin	a_i	b_i	c_i	d_i	a_i	c_i	c_i'	d_i
1	97.24	-0.46	12.00	-8.91	40.86	26.77	-29.59	-45.75
2	107.22	1.15	0.59	-3.95	26.58	14.73	58.46	-21.25
3	104.97	2.96	-5.53	-8.77	19.34	2.28	100.00	0.25
4	102.39	5.59	-13.95	-13.90	13.25	-1.39	124.79	15.66
5	100.71	5.94	-22.75	-23.74	14.47	-5.09	160.09	9.13
6	106.42	3.83	-36.15	-28.83	19.76	-3.88	154.61	-19.21
7	141.88	1.90	-53.24	-14.03	28.39	-9.67	151.58	-69.39
8	152.23	0.35	-45.27	-7.98	42.91	-19.62	130.80	-164.08

Model formulation. Diffuse illuminance may be derived from diffuse irradiance and the sky condition parameters through eqn (7). This is given below:

$$dh = Dh[a_i + b_i W + c_i \cos(Z) + d_i Ln(\Delta)] \quad (7)$$

The coefficients of eqn (7), which were derived by least-square fitting of over 20,000 points are given in Table 4. Coefficients for the two highest ϵ bins were derived from fixed shadowband diffuse irradiance and illuminance measurements available in Albany only: although diffuse measurements with standard shadowbands are inherently less accurate than those obtained by global and direct difference, this is not the case for clear day diffuse luminous efficacy measurement: in this case, the diffuse component is small compared to

Table 5. Luminous efficacy and zenith luminance model RMS and mean bias error as a function of insolation conditions and location

	INSOLATION CONDITIONS							
	Overcast		Intermededite		Clear		All events	
SITE	MBE	RMSE	MBE	RMSE	MBE	RMSE	MBE	RMSE
Global Illuminance Prediction Model								
Albany	0.3%	5.0%	0.5%	3.3%	0.3%	2.4%	0.4%	3.4%
Farmingdale	1.2%	3.4%	1.4%	3.0%	1.2%	2.7%	1.2%	3.2%
Queens	-1.3%	3.5%	-1.3%	2.7%	-1.2%	2.4%	-1.2%	2.9%
Glens Falls	-0.3%	4.9%	-0.6%	4.0%	-0.6%	3.3%	-0.6%	4.1%
Oswego	-0.5%	2.5%	0.9%	2.5%	1.2%	1.9%	0.5%	2.5%
Geneva	0.1%	5.7%	-1.5%	3.7%	1.6%	3.2%	0.7%	4.3%
Diffuse Illuminance Prediction Model								
Albany	0.2%	5.1%	0.8%	7.2%	0.9%	13.7% (7%)*	0.6%	8.4% (6%)*
Farmingdale	1.1%	3.5%	1.5%	6.1%	1.9%	11.1%	1.4%	6.7%
Queens	-1.1%	3.5%	-1.1%	6.0%	-1.3%	12.1%	-1.1%	7.4%
Glens Falls	-0.3%	5.2%	-0.8%	8.7%	-0.5%	17.3%	-0.5%	10.6%
Oswego	-0.6%	2.7%	0.8%	5.0%	-1.4%	11.4%	-0.8%	5.9%
Geneva	0.4%	6.1%	3.8%	9.1%	3.5%	10.2%	2.3%	8.7%
* Value derived from fixed shadowband measurements								
Direct Illuminance Prediction Model								
Albany	-----	----	1.0%	10.7%	0.7%	5.7%	0.7%	7.1%
Farmingdale	-----	----	1.2%	10.7%	1.0%	4.3%	1.0%	5.8%
Queens	-----	----	-1.4%	10.0%	-0.9%	4.2%	-1.0%	5.6%
Glens Falls	-----	----	-1.6%	12.8%	-1.3%	5.3%	-1.4%	7.4%
Oswego	-----	----	1.9%	9.8%	1.3%	4.0%	1.5%	5.9%
Geneva	-----	----	-4.3%	14.0%	0.8%	4.5%	-1.6%	9.5%
Zenith Luminance Prediction Model								
Albany	3.2%	19.0%	-1.1%	24.0%	1.0%	24.1%	0.4%	21.5%
Farmingdale	3.0%	19.1%	-2.3%	24.0%	2.0%	30.2%	0.8%	22.9%
Queens	-2.5%	17.6%	1.3%	21.9%	0.3%	28.2%	-1.2%	21.8%
Glens Falls	-3.1%	25.1%	4.9%	29.4%	3.6%	26.3%	-0.9%	30.6%
Oswego	-9.0%	23.9%	1.1%	24.9%	1.6%	23.8%	0.3%	24.6%

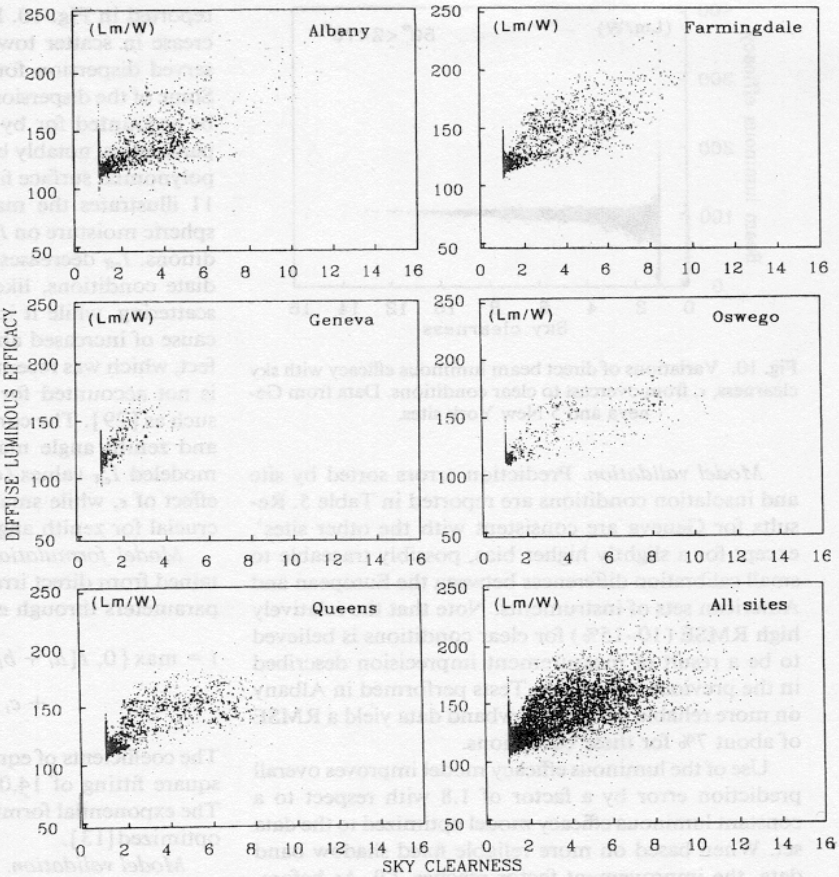

Fig. 7. Variations of diffuse luminous efficacy with sky clearness, ϵ, for five locations.

the direct and global components. If diffuse is obtained by difference of the latter, a small relative error in any one of those will result in a potentially large relative error in the diffuse value; moreover, since diffuse luminous efficacy is the ratio of two such differences, the measurement error may reach unacceptable levels. On the other hand, when deriving luminous efficacy from shadowband measurements, the initial source of error has a tendency to "self-correct" since the shadowband blocks an identical portion of the sky for both irradiance and illuminance; aside from circumsolar spectral differences, the shadowband error is canceled out by ratioing the two quantities.

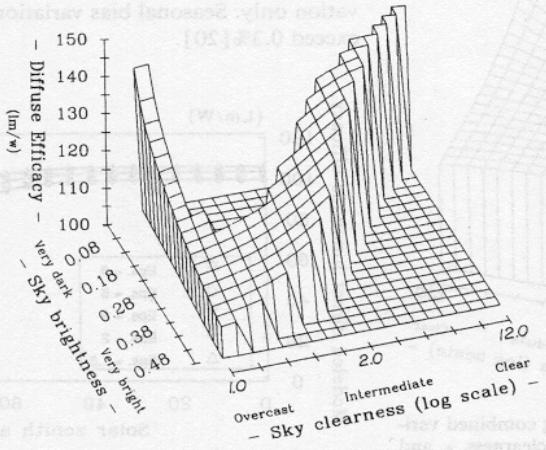

Fig. 8. Best-fit polynomial surface showing combined variations of diffuse luminous efficacy with ϵ and Δ at Z and Td = constant. (see note in Fig. 5.).

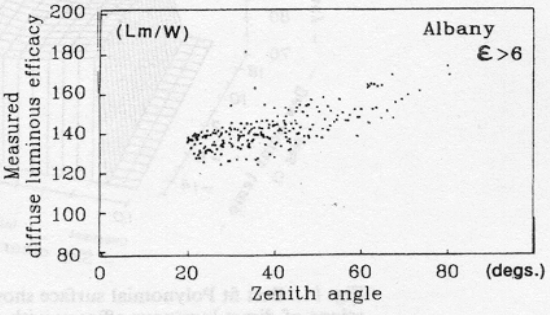

Fig. 9. Variations of diffuse luminous efficacy with solar zenith angle for very clear conditions. Data from Albany, NY (fixed shadowband measurements).

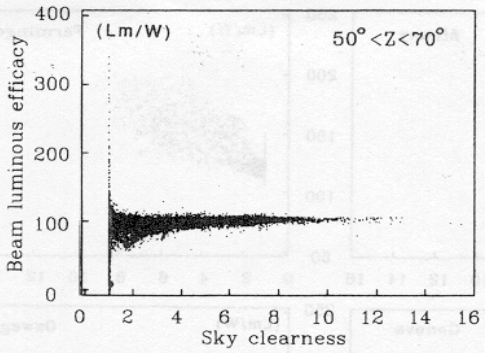

Fig. 10. Variations of direct beam luminous efficacy with sky clearness, ϵ, from overcast to clear conditions. Data from Geneva and 5 New York sites.

Model validation. Prediction errors sorted by site and insolation conditions are reported in Table 5. Results for Geneva are consistent with the other sites', except for a slightly higher bias, possibly traceable to small calibration differences between the European and American sets of instruments. Note that the relatively high RMSE (10–15%) for clear conditions is believed to be a result of measurement imprecision described in the previous paragraph. Tests performed in Albany on more reliable fixed shadowband data yield a RMSE of about 7% for these conditions.

Use of the luminous efficacy model improves overall prediction error by a factor of 1.8 with respect to a constant luminous efficacy model optimized to the data set. When based on more reliable fixed shadow band data, the improvement factor reaches 2.9. As before, no seasonal bias is detected. Existing winter–summer differences are well accounted for by the surface dew point input (coefficient b_i in eqn (7)).

3.1.3 *Direct irradiance to illuminance conversion.*

Key observations. Observed variations of direct luminous efficacy, I_{eff}, with sky clearness at $Z \sim$ cst are reported in Fig. 10. Except for an understandable increase in scatter toward overcast conditions, the observed dispersion for the six sites is remarkably low. Some of the dispersion for intermediate conditions may be accounted for by varying conditions of the other parameters, notably by the dew point temperature. The polynomial surface fitted to all data and plotted in Fig. 11 illustrates the markedly different effect of atmospheric moisture on I_{eff} for clear and intermediate conditions. I_{eff} decreases with increasing Td for intermediate conditions, likely because of enhanced aerosol scattering, while it increases for clear conditions, because of increased absorption in the infrared. This effect, which was recently reported and discussed in [13] is not accounted for in physically based approaches such as [29]. The combined influence of sky clearness and zenith angle may be assessed in Fig. 12, where modeled I_{eff} values (eqn (8)) have been plotted: The effect of ϵ, while small for low zenith angles becomes crucial for zenith angles in excess of 70°.

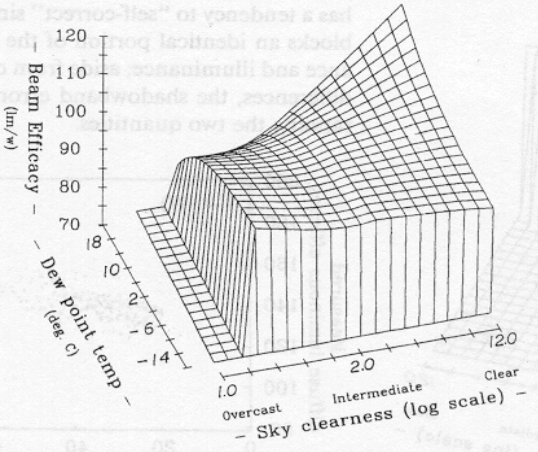

Fig. 11. Best fit Polynomial surface showing combined variations of direct luminous efficacy with sky clearness, ϵ, and surface dew point temperature, Td. (Note that the surface was not plotted for low ϵ values where direct luminous efficacy becomes a meaningless quantity).

Model formulation. Direct illuminance, i, is obtained from direct irradiance, I, and the sky condition parameters through eqn (8).

$$i = \max\{0, I[a_i + b_i W + c_i \exp(5.73\, Z - 5) + d_i \Delta]\} \quad (8)$$

The coefficients of eqn (8), which were derived at least-square fitting of 14,000 points are given in Table 4. The exponential formulation for Z had been previously optimized [13].

Model validation. Prediction errors are reported in Table 5. Performance is consistent at all sites, with slightly more dispersion observed in Geneva for intermediate conditions: Possible causes are instrumentation differences, and a possibly different W-Td relationship at the European location.

Overall, the present model results in an improvement by a factor of 3 over a constant luminous efficacy model optimized to the present data set and by a factor of 1.4 over a model that would account for solar elevation only. Seasonal bias variations are found not to exceed 0.3% [20].

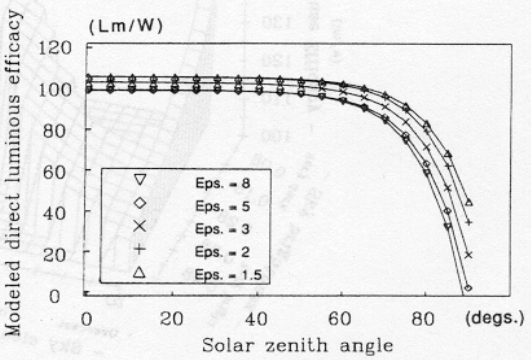

Fig. 12. Variations of modeled direct beam luminous efficacy with solar zenith angle for different values of sky clearness, ϵ. Data from five New York sites.

3.2 *Diffuse irradiance and illuminance on tilted surfaces modeling*

These models estimate the total (integrated) sky diffuse irradiance/illuminance received by a surface tilted from the horizontal (e.g., a window). The ground-reflected diffuse component may be added to obtain the total hemispheric diffuse radiation on a slope. This is not treated here but in a separate paper by the authors[30]. Output data are suitable for most energy gain calculations (e.g., solar[31], HVAC[3]) and for simple daylighting calculations (e.g., [32]). More complex daylighting applications that require an actual knowledge of the light source angular distribution should instead rely on the models presented in Section 3.3.

Both models are based on the anisotropic diffuse model developed by Perez *et al.*[33] and commonly referred to as the Perez model. This has been considerably simplified since the original version[16] while conserving its original representation of the sky dome as an isotropic background upon which are superimposed a circumsolar and horizon/zenith effects; these effects are, respectively, simulated by a point source at the sun's position and a linear source at the horizon; the latter can be either a positive or negative source signifying respectively horizon and zenith brightening.

Model formulation. The model governing equation for both illuminance and irradiance is

$$Xc = Xh[(1 - F_1)(1 + \cos S)/2 + F_1 a/b + F_2 \sin S] \quad (9)$$

where Xc and Xh are, respectively, the tilted and horizontal diffuse value of either illuminance or irradiance, S is the considered surface's slope, F_1 and F_2 are coefficients expressing the degree of circumsolar and horizon/zenith anisotropy respectively; they are functions of the sky condition. The terms a and b are given below:

$$a = \max(0, \cos\theta) \quad \text{and} \quad b = \max(0.087, \cos Z)$$

where θ is the incidence angle of the sun on the considered slope.

3.2.1 *Irradiance model.* The irradiance version of the model has been extensively validated. In its original version, it was reviewed and selected by the International Energy Agency[34]. Recent research and cooperation programs[35] allowed for optimizing and testing the model against data from 13 sites.

Model coefficients. The variations of horizon and circumsolar brightening coefficients F_1 and F_2 with insolation conditions have been observed to be consistent from site to site[17,20]. Some of the key features are presented in Fig. 13 where variations with ϵ for a given zenith angle range have been reported. These features include gradual increase of the circumsolar coefficient from a value of 0 for overcast conditions to about 0.6 for intermediate-to-clear conditions ($\epsilon \approx 2$–3) followed by a marked decrease toward very clear conditions. For the horizon coefficient, an increase from a negative value for overcast conditions to a positive value for clear conditions is noted. These observations are consistent with the physical processes affecting solar radiation atmospheric transfer: the circumsolar peak for intermediate conditions corresponds to a maximum in forward scattering by thin/scattered cloud and/or high aerosol content, the subsequent decrease toward clear conditions is indicative of a decrease in atmospheric aerosol content. The negative value for F_2 is traceable to a relative brightening of the zenithal region for overcast conditions the physical nature of which is well understood[36], the positive value for clear skies is to be expected from Rayleigh scattering in an homogeneous nonabsorbing atmosphere. However, perhaps more remarkable than basic agreement with understood physical processes, is the fact that the observed variation patterns are continuous and exhibit low dispersion over the complete range of insolation conditions and that indeed, the so-called intermediate skies exhibit very predictable site-independent anisotropic features, when parameterized as proposed, despite the possible combinations of cloud type/height and turbidity for these conditions.

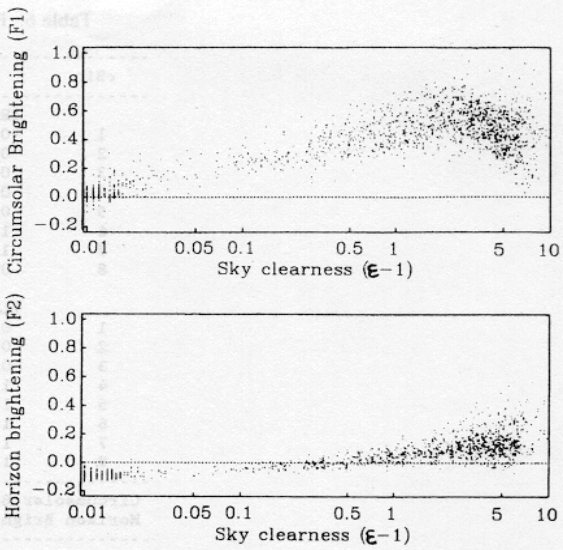

Fig. 13. Variations of circumsolar and horizon brightening coefficients with sky clearness, ϵ at $Z \sim$ constant (45°–55°). Data from Albuquerque, Pheonix, Los Angeles, Cape Canaveral, and Osage.

The recommended set of coefficients is based on data from Albany, Geneva, Los Angeles, Albuquerque, Phoenix, Cape Canaveral, Osage, Trappes, and Carpentras. These are given in Table 6. This set differs slightly from that presented at an earlier stage in Perez *et al.*[17]. The continuous evolution of coefficients may be related to their sensitivity to the range of the data from which they are derived. However, the validation results reported in Table 7 demonstrate that the coefficients have now achieved an asymptotic level of optimization and that the choice between the current and previous sets is far from critical.

Table 6. Perez model coefficients for irradiance and illuminance

ϵBin	F_{11}	F_{12}	F_{13}	F_{21}	F_{22}	F_{23}
	IRRADIANCE COEFFICIENTS					
1	-0.008	0.588	-0.062	-0.060	0.072	-0.022
2	0.130	0.683	-0.151	-0.019	0.066	-0.029
3	0.330	0.487	-0.221	0.055	-0.064	-0.026
4	0.568	0.187	-0.295	0.109	-0.152	-0.014
5	0.873	-0.392	-0.362	0.226	-0.462	0.001
6	1.132	-1.237	-0.412	0.288	-0.823	0.056
7	1.060	-1.600	-0.359	0.264	-1.127	0.131
8	0.678	-0.327	-0.250	0.156	-1.377	0.251
	ILLUMINANCE COEFFICIENTS					
1	0.011	0.570	-0.081	-0.095	0.158	-0.018
2	0.429	0.363	-0.307	0.050	0.008	-0.065
3	0.809	-0.054	-0.442	0.181	-0.169	-0.092
4	1.014	-0.252	-0.531	0.275	-0.350	-0.096
5	1.282	-0.420	-0.689	0.380	-0.559	-0.114
6	1.426	-0.653	-0.779	0.425	-0.785	-0.097
7	1.485	-1.214	-0.784	0.411	-0.629	-0.082
8	1.170	-0.300	-0.615	0.518	-1.892	-0.055
Circumsolar Brightening Coefficient				$F_1 = F_{11} + F_{12}*\Delta + F_{13}*Z$		
Horizon Brightening Coefficient				$F_2 = F_{21} + F_{22}*\Delta + F_{23}*Z$		

Model validation. Model resultant RMS and mean bias error for all sites studied are reported in Table 8. These are sorted as a function of surface orientation and compared to that of two reference models: the isotropic and the Hay models [37]. Overall RMS error is kept at ≈ 15 W/m^2, as opposed to 39 and 25 W/m^2 for the two reference models.

Site dependency may be assessed by looking at Table 7 where overall RMS errors have been reported, sorted by site and origin of coefficient set. It can be seen (i) that performance is consistent at all sites, and that (ii) for all but one case, (Osage, KS), coefficients derived from any one site yield a better performance than the reference models—the Osage exception may be traced to the lack of experimental data for certain insolation conditions and the resulting distortion from the coefficients fitted to those data.

3.2.2 *Illuminance model.* The model formulation is identical to that of the irradiance model (eqn (9)), with the exception that horizontal diffuse illuminance is the first term on the right-hand side of eqn (9). This is obtained from diffuse irradiance using eqn (7).

Model coefficients. Concerning the coefficients, a distinct illuminance set is recommended to account for the difference between daylight and radiant power anisotropy. The recommended illuminance set is provided in Table 6. This was derived from five northeast U.S. sites. The use of a distinct set is clearly justified by the validation results presented below. Some qualitative differences between irradiance and illuminance coefficients are shown in Fig. 14: Observed variations with ϵ at $Z \approx$ cst are compared for two time-coincident sets. Differences are small but two distinctions merit a comment: (i) the decrease of circumsolar brightening toward very clear skies is less pronounced for the illluminance component; and (ii) horizon darkening (i.e., zenith brightening) for overcast conditions is more pronounced for the irradiance component—a consequence of water vapor absorption (see [20]).

Model validation. Model performance is reported in Table 8, in terms of orientation-dependent RMSE and MBE. Four versions of the model are presented and compared to the two reference models. Versions 1, 2, and 3 use measured horizontal diffuse illuminance as input for eqn (9) but use three different sets of coefficients, respectively: (i) the recommended illuminance

Table 7. Tilted diffuse irradiance model composite RMSE as a function of location and origin of coefficients

MODEL	PEREZ												HAY	ISO
Coefficients	Phoen. El Mte		Osage Albuq.		C.Can. SNLA		Alby USA		Fra.		Geneva US+Fr.		-	-
	ALL											ALL		
LOCATION	Five-Orientation Composite RMSE (W/m)													
Phoenix, AZ	13	15	64	15	20	13	18	15	22	17	16	16	20	34
El Monte, CA	15	13	48	17	17	14	18	15	19	16	17	17	23	45
Osage, KS	17	16	13	20	18	15	20	18	20	18	17	17	28	46
Albuquerque, NM	13	14	50	12	15	13	16	13	17	14	15	14	20	33
C.Canaveral, FL	14	17	36	14	12	14	16	14	19	17	17	17	23	34
ALL ABOVE SITES	14	15	51	16	17	14	17	15	19	16	16	16	22	38
Albany (SEMTS)	17	16	42	16	17	16	13	14	15	13	14	13	24	36
ALL ABOVE SITES	16	16	45	16	17	15	14	14	16	14	15	14	23	36
Trappes & Carp.	20	20	21	20	19	19	16	17	15	16	17	16	28	43
ALL ABOVE SITES	17	17	43	17	17	17	15	15	16	15	16	15	25	38
Geneva, Switz.	19	17	23	18	18	18	17	16	17	16	15	15	24	39
ALL SITES	19	18	41	18	18	17	16	16	17	15	16	15	25	39

Table 8. Overall RMSE and mean bias error for tilted diffuse irradiance and illuminance models

Surface Orientation	Mean Global Irradiance (W/m^2)	IRRADIANCE MODEL ERROR (W/m^2) PEREZ 1 RMSE	PEREZ 1 MBE	ISOTROPIC RMSE	ISOTROPIC MBE	HAY RMSE	HAY MBE
90° North	64	11	3	32	18	24	1
90° East	174	17	-2	43	-7	29	-9
90° South	230	16	0	38	-17	25	-10
90° West	173	17	1	43	-6	28	-7
45° South	396	14	-1	36	-22	22	-11
Composite error		15	2	39	17	25	9

Surface Orientation	Mean Global Illumin. (100*lux)	ILLUMINANCE MODEL ERROR (100 * LUX) PEREZ 1 RMSE	PEREZ 1 MBE	PEREZ 2 RMSE	PEREZ 2 MBE	PEREZ 3 RMSE	PEREZ 3 MBE	PEREZ 4 RMSE	PEREZ 4 MBE	ISOTROPIC RMSE	ISOTROPIC MBE	HAY RMSE	HAY MBE
90° North	71	12	2	12	2	14	6	11	2	38	22	30	3
90° East	160	17	-1	19	0	19	2	18	-1	51	0	33	-5
90° South	269	16	-1	18	-2	19	-1	19	-2	61	-30	34	-12
90° West	173	17	3	20	4	20	6	18	-3	50	-5	32	-2
Composite error		16	2	18	2	18	4	17	5	50	19	33	7

PEREZ 1: Illuminance coef. PEREZ 2: Dependent Irradiance Coef.
PEREZ 3: Independent Irradiance Coef.
ISOTROPIC, HAY, PEREZ 1, 2 and 3: Diffuse Illuminance Input
PEREZ 4: Operational Model -- Illum. coef. plus diffuse irradiance input --

set in Table 6; (ii) a set of irradiance coefficients derived from the same data; and (iii) the independent irradiance set recommended in Table 6. The fourth version is the operational version of the model which combines eqn (7) to derive horizontal diffuse illuminance and the illuminance coefficients.

Results show that performance degradation from an illuminance coefficient set to an irradiance set derived from the same data exceeds that from the latter to an independently derived irradiance set. This observation tends to justify the recommendation for a distinct set of coefficients for the illuminance model. Results also show that the operational version of the model, which uses only the irradiance data as input, does not yield significant performance deterioration. In summary, the prediction of diffuse illuminance on a tilt is as accurate overall as that of diffuse irradiance.

3.3 *Sky luminance modeling*

3.3.1 *Zenith luminance prediction model.* Zenith luminance is treated distinctly because (i) it is a design quantity of interest by itself, and because (ii) this is

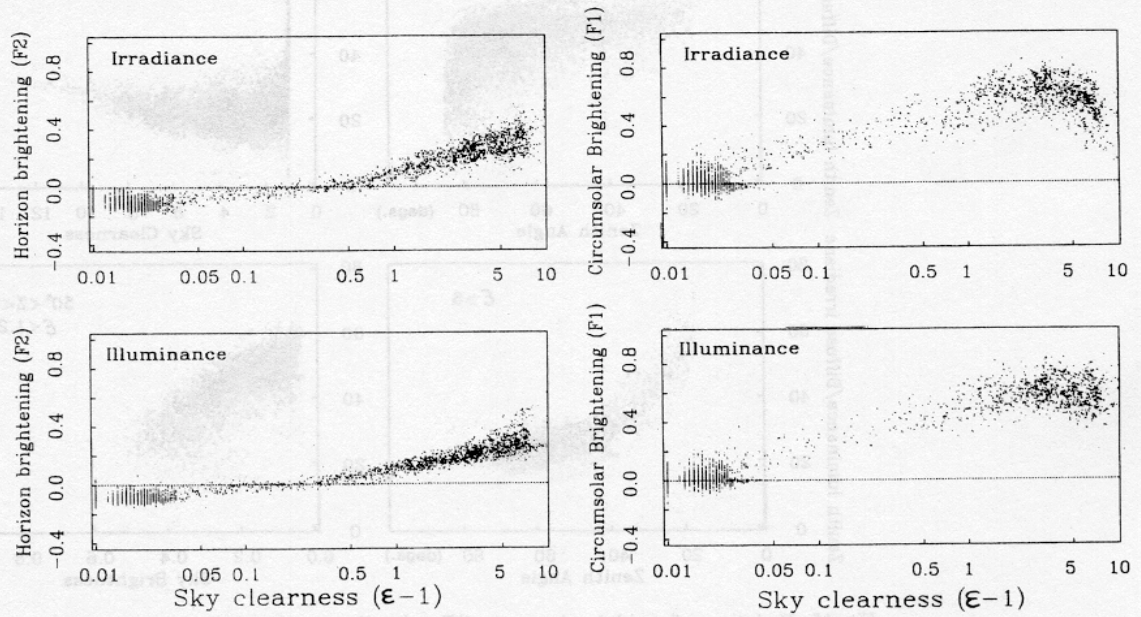

Fig. 14. Compared variations of circumsolar and horizon brightening coefficients with ϵ for irradiance and illuminance ($45° < Z < 55°$). Data from five New York sites.

the main input quantity of CIE standard angular luminance distribution models [5–7].

Key observations. A "pseudo luminous efficacy," L_{eff}, is defined as the ratio of zenith luminance to diffuse irradiance. Observed variations of L_{eff} with selected sky conditions parameters are presented in Fig. 15. This includes (i) variations with ϵ at $Z \approx$ cst, (ii) variations with Δ for overcast conditions at $Z \approx$ cst, (iii) variations with Z for average overcast conditions ($0.1 < \Delta < 0.3$), and (iv) variations with Z for clear sky conditions. Plots are based on all data available from the five New York sites.

Variations are well defined and are in general agreement with radiative transfer expectations. As noted before, the continuous pattern across all insolation conditions is remarkable. The strong decrease with increasing sky brightness for overcast conditions is most interesting: It indicates that standard CIE overcast description [5] with it bright zenithal region is valid only for dark overcast skies.

Model formulation. Zenith luminance, Lvz, is obtained from diffuse irradiance, Dh, and the sky condition parameters through eqn (10).

$$Lvz = Dh[a_i + c_i \cos Z + c_i' \exp(-3Z) + d_i\Delta] \quad (10)$$

The coefficients of eqn (10), which were derived by least-square fitting of 22,000 points may be found in Table 4. Given the zenith angle validation domain ($17° < Z < 85°$) care should be used outside those bounds. Notably, the authors recommend use of $Z' = \max(Z, 0.6)$ instead of Z for the lowest ϵ bin in eqn (10) and to view results for $Z < 17°$ with caution until further validation.

Model validation. Mean bias and RMS prediction errors are reported in Table 5, in percentage of mean value terms. Differences between sites studied are negligible as can be seen from the overall bias errors which are kept below 1% (this is also found to be season independent [20]). Relative RMS errors are larger than that obtained for the other type of models described above; this is to be expected because of the high variability that may occur in a confined region of the sky dome for all but extremely clear and dark overcast conditions. In absolute terms, RMS errors range from 0.7 kcd/m^2 for clear conditions to 1.5 kcd/m^2 for bright intermediate skies. Comparison for clear sky conditions against existing models proposed by Dogniaux [38] and Karayel *et al.* [39] indicates 2 : 1 performance gain [18]—note that these models, operational for clear sky conditions only are turbidity dependent, hence, require the same input information as the present model.

3.3.2 *Sky luminance angular distribution model.* Sky luminance distribution is the "ultimate" daylight availability quantity for daylighting calculations. Modern design software [1] is now able to effectively use sky maps and beam illuminance to precisely model

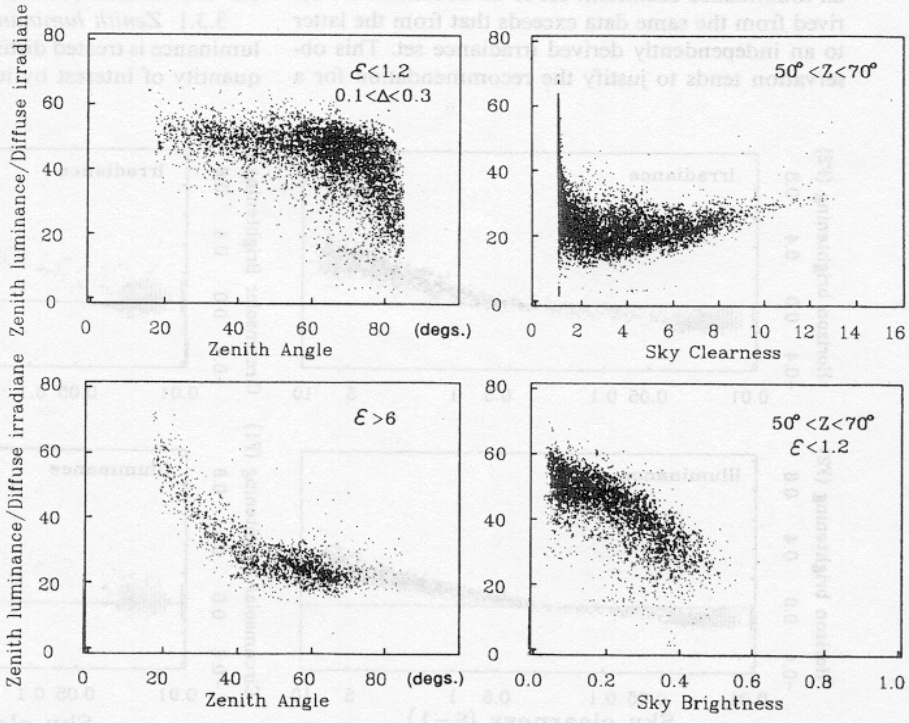

Fig. 15. Variations of zenith luminance-to-diffuse irradiance ratio with (a) Solar zenith angle for overcast conditions. (b) Sky clearness, ϵ, for a limited zenith angle range. (c) Solar zenith angle for very clear conditions. (d) Sky Brightness, Δ, for overcast conditions. (Data from five New York sites).

light distribution in complex interior spaces with complex apertures and outdoor obstructions. Because of the limited coverage of sky luminance distribution available for this study (five points in the sky dome) and the possibility for resulting model distortion, new model development was not undertaken at this time. Rather, the study focused on evaluating and developing operational versions of existing standard models. More complete model development and validation of other nonstandard approaches [e.g., 15,40] will occur in the foreseeable future using the large worldwide sky luminance distribution data base the CIE's International Daylighting Measurement Year[41] is expected to produce.

Model formulation. A combination of CIE skies is proposed as an interim operational model. These are (i) the standard CIE overcast sky[5], (ii) the standard CIE clear sky[6], (iii) a high turbidity formulation of the latter[7], and (iv) a realistic formulation for intermediate skies proposed by a CIE working committee[7].

The model is formulated as follows:

$$Lvc = Lvz * \psi \tag{11}$$

where ψ is a geometrical factor depending on the solar position, and the considered luminance direction. It is obtained by interpolation of four CIE formulations [eqs (12), (13), (14), and (15)] given below.

Clear sky formulation

$$\psi_{cs} = \Phi(\gamma) f(\zeta) / [\Phi(\pi/2) f(Z)] \tag{12}$$

where

$\Phi(X) = 1 - \exp(-0.32/\sin X)$
$f(X) = 0.91 + 10\exp(-3X) + 0.45(\cos X)^2$
γ: considered point elevation in radians
ζ: direct beam vs. considered direction angle in radians
Z: solar zenith angle in radians

Clear turbid (polluted) sky

$$\psi_{ts} = \Phi(\gamma) f'(\zeta) / [\Phi(\pi/2) f'(Z)] \tag{13}$$

where $f'(X) = 0.856 + 16\exp(-3X) + 0.3(\cos X)^2$

Intermediate sky

$$\psi_{is} = a(\gamma_s, \gamma)\exp[\zeta b(\gamma_s, \gamma)] / \{a(\gamma_s, \pi/2)\exp[Zb(\gamma_s, \pi/2)]\} \tag{14}$$

where

$$\gamma_s = \pi/2 - Z,$$

$a(X, Y) = [1.35\{\sin(3.59Y - 0.009) + 2.31\} \times \sin(2.6X + 0.316) + Y + 4.799]/2.326,$

$b(X, Y) = -0.563[(Y + 1.059)(X - 0.008) + 0.812].$

Overcast sky

$$\psi_{os} = (1 + 2\sin\gamma)/3 \tag{15}$$

The linear interpolation of the four terms is a function of the sky condition components Δ and ϵ. Limits are determined by correspondence between each CIE standard's distribution profiles and experimentally derived coefficients of the Perez diffuse illuminance model (Section 3.2.2). For instance, the intermediate CIE sky, which features a strong circumsolar effect, but no horizon brightening, is set at $\epsilon = 1.2$ and $\Delta = 0.5$—this corresponds to a large value of F_1 at $F_2 = 0$ in the illuminance model (see Fig. 14).

Specifically ψ is obtained from

If $\epsilon \leqq 1.2$ then

$$\psi = (1 - a)\psi_{os} + a\psi_{is}, \tag{16}$$

where

$a = \min\{1, \max[0, (\epsilon - 1)/0.2, (\Delta - 0.05)/0.4]\},$

If $1.2 < \epsilon \leqq 3$ then

$$\psi = (1 - b)\psi_{is} + b\psi_{ts},$$

where

$$b = (\epsilon - 1.2)/1.8,$$

If $\epsilon > 3$ then

$$\psi = (1 - c)\Psi_{ts} + c\Psi_{cs},$$

where

$$c = \min[1, (\epsilon - 3)/3].$$

Model evaluation. Two versions are evaluated here, one that uses measured Lvz as input in eqn (11) and an "operational version" that combines eqns (11) and (10) and uses only an irradiance input. Performance is compared to that of two simpler models: (i) an isotropic sky model that assumes constant luminance throughout the sky dome; and (ii) an anisotropic equivalent sky luminance model; the latter assumes that luminance at any given point in the sky dome is equal to the mean luminance viewed by a tilted plane facing that point—mean luminance is obtained by dividing the diffuse illuminance value from eqn (9) by the sky Lambertian solid angle viewed by the plane.

Validation data consist of measured luminance values at 45° elevation in four azimuths. Note that in this case, validation is totally independent since there is no relationship between test experimental data and model derivation. Observed relative (%) differences between modeled and all available measured values in Albany are plotted as a function of sky clearness in

Fig. 16. It is apparent that the CIE combination models do a better job than the two simpler models to predict luminance at 45° elevation in the sky vault. The tendency of the equivalent luminance anisotropic sky model to overestimate for clear conditions is simply caused by the fact that this incorporates horizon brightening (seen by the tilted plane) whereas the test positions are above the luminance enhancement region. Use of modeled rather than measured input for the CIE formulation does not result in apparent performance deterioration.

Quantitative validation summaries (RMSEs and MBEs) are given in Table 9 for each site, model and luminance direction. It is noteworthy to remark that the model that uses modeled zenith luminance from irradiance is slightly more accurate than the one that relies on measured zenith luminance. This is understandable because the diffuse irradiance input contains information from the entire sky whereas zenith luminance is a point measurement. Overall, use of this model results in a 1.6 : 1 performance improvement over the uniform sky and a 1.25 : 1 improvement over the anistropic equivalent luminance sky for the region of the dome presently under investigation.

Recommendation. Closer scrutiny of results indicates that it is likely that luminance distribution model performance may be improved in the future. Table 10 reports model MBEs and RMSEs for Farmingdale, sorted by sky condition, solar zenith angle and luminance direction for the selected model. The distinct bias pattern would indicate that a better fit to the data is possible. This task cannot be undertaken with the present luminance data since a fit to that data (only five directions in the sky vault) could result large distortions for other positions in the sky.

For the present, the level of precision achieved in this independent test would warrant recommendation of the proposed CIE interpolation method for applications as an "all-weather" operational skylight distribution model. Note that, in practice, when a map of the sky is generated the resultant overall bias can be totally eliminated by simple normalization as shown in eqn (17).

$$L'vc = Lvc\left[dh \Big/ \left(\int_{\text{all-sky}} Lvc \sin\gamma d\Omega\right)\right] \quad (17)$$

The normalized luminance, $L'vc$, at any given point is equal to the luminance obtained from eqn (11) multiplied by the ratio between diffuse illuminance, dh, calculated from eqn (7), and the same quantity ob-

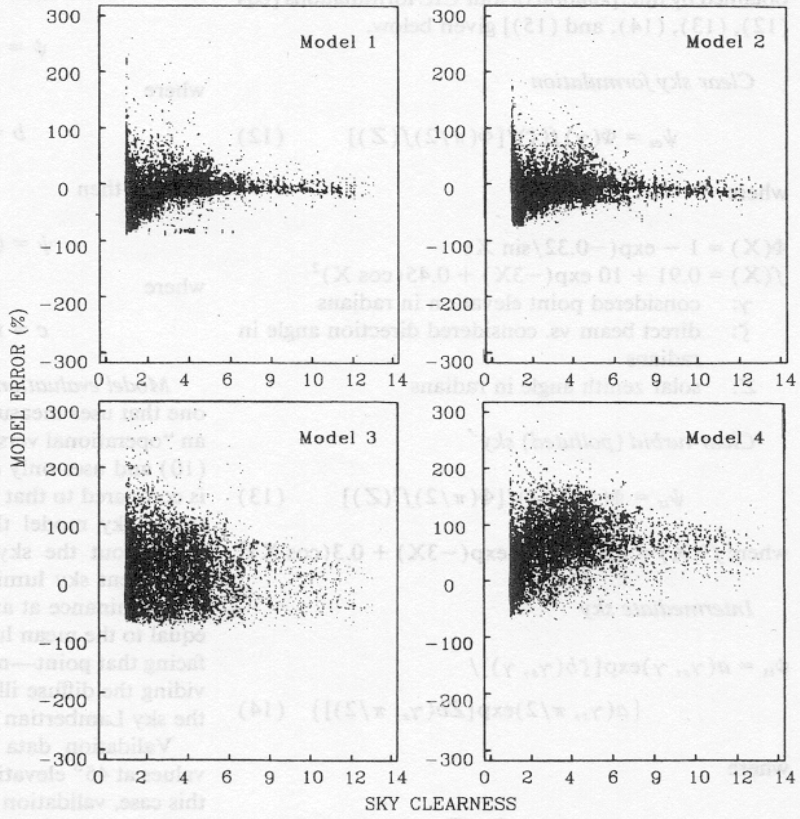

Fig. 16. Relative difference between measured and modeled luminance at four points in the sky dome (Model 1: eqn (11) + measured zenith luminance input; Model 2: eqn (11) + horizontal diffuse irradiance input; Model 3: Isotropic Sky; Model 4: Anisotropic sky equivalent luminance). Data from five New York sites.

Table 9. Validation performance summary for luminance distribution models

SITE	LUMINANCE DIRECTION	NO. OF EVENTS	MEAN (cd/m^2)	MODEL ERROR (cd/m^2) MODEL 1 RMSE	MODEL 1 MBE	MODEL 2 RMSE	MODEL 2 MBE	MODEL 3 RMSE	MODEL 3 MBE	MODEL 4 RMSE	MODEL 4 MBE
Albany	N. 45°	5628	3666	992	-157	1008	-226	1683	642	1650	832
Albany	E. 45°	5368	4697	1587	-481	1581	-558	2466	-400	1934	497
Albany	S. 45°	5182	6462	3066	-785	2831	-870	4278	-2282	2958	-86
Albany	W. 45°	3610	3957	1231	-368	1200	-427	1532	-311	1796	822
Farmin.	N. 45°	5956	4086	1098	-225	1126	-274	1885	536	1801	759
Farmin.	N. 45°	5786	5067	1929	-290	1904	-274	3076	-472	2331	651
Farmin.	S. 45°	5490	6662	2645	-616	2452	-628	4249	-2169	2864	100
G. Fls.	N. 45°	1259	2154	889	-459	946	-449	1311	733	1160	768
G. Fls.	E. 45°	1204	2542	892	-116	891	-104	1319	279	2068	1637
Oswego	N. 45°	1710	3211	832	-358	859	-354	1290	458	1016	342
Oswego	E. 45°	1724	4025	1431	-562	1451	-554	1778	-360	1581	504
Oswego	S. 45°	1591	5578	2802	-835	2559	-842	3735	-2032	2462	-18
Queens	N. 45°	6949	3871	1143	-51	1080	-13	1865	856	1944	1210
Queens	E. 45°	6520	5359	2109	-466	1999	-385	3438	-697	2419	655
Queens	S. 45°	6480	6934	2825	-862	2645	-791	4555	-2346	2691	89
ALL	COMPOSITE	67883	----	1866	442	1772	486	2816	972	2144	598

Model 1: Equation 11 with measured zenith luminance input
Model 2: Equation 11 with diffuse irradiance input (through equation 7)
Model 3: Isotropic sky
Model 4: Equivalent luminance, anisotropic sky

tained by integration of the luminance points calculated from eqn (11).

4. CONCLUSIONS

This paper has presented a set of models designed to generate a comprehensive array of energy/daylight quantities relevant to the design and optimization of solar energy systems and building structures and components. All models share a common operating methodology in the sense that (i) they are designed to span all conditions from overcast to clear, and (ii) they rely on the same input data and insolation conditions pa-

Table 10. Luminance model RMS and mean bias error as a function of orientation and insolation conditions in Farmingdale

SOLAR ZENITH ANGLE RANGE	Overcast MBE cd/m^2	Overcast RMSE cd/m^2	Overcast mean cd/m^2	Intermediate MBE cd/m^2	Intermediate RMSE cd/m_2	Intermediate mean cd/m^2	Clear MBE cd/m^2	Clear RMSE cd/m2	Clear mean cd/m^2
INSOLATION CONDITIONS									
NORTH 45° ORIENTATION									
0°-35°	-545	1823	9327	995	3170	8575	-102	940	3548
35°-50°	-148	1352	7578	-150	1854	6577	-160	927	2599
50°-65°	-365	968	5090	-437	1390	4429	-292	598	2154
65°-75°	-389	789	3410	-455	895	3085	-219	381	1780
75°-85°	-316	514	1830	-432	572	1774	-272	338	1241
0°-85°	-344	1108	5195	-178	1703	4729	-230	644	2161
EAST 45° ORIENTATION									
0°-35°	-532	2262	9988	722	3024	12344	210	1970	5480
35°-50°	102	1869	8137	-245	3023	9041	-7	1382	4011
50°-65°	-384	1784	5462	-995	3245	6524	46	1215	3325
65°-75°	-805	2007	4075	-1506	2854	4951	218	906	2704
75°-85°	-539	1027	2105	-804	1331	2357	-13	497	1808
0°-85°	-446	1832	5634	-677	2850	6838	86	1215	5046
SOUTH 45° ORIENTATION									
0°-35°	-1499	3134	11414	-1843	4199	21224	289	2418	10279
35°-50°	-981	2731	9853	-1892	4708	15329	542	1786	6272
50°-65°	-980	2497	6624	-2891	5267	10952	519	1514	5684
65°-75°	-733	1597	4114	-1119	2344	5238	297	827	3383
75°-85°	-243	515	1790	-411	633	1993	-68	233	1487
0°-85°	-859	2230	6334	-1752	3957	10359	339	1441	5046

rameterization—input is compatible with currently available data and with that likely to be provided by a new generation of low cost/low maintenance instruments.

The models have been extensively validated using data representative from various climatic environments. These range from maritime to high altitude deserts for the irradiance models and from temperate maritime to continental for the daylight availability models. For each model, a noticeable performance improvement is found over existing methods that accomplish the same task.

The experimental/statistical approach used to derive the models can be considered both as an asset and a liability. On the asset side, the experimental approach allows for simply delineating particular configurations, which are far from straightforward in terms of radiation transfer calculations: The delineation of intermediate cases between very clear and totally overcast extremes is an example (e.g., the combined effect of surface dew point and atmospheric clearness effects on direct beam luminous efficacy); the observation of well-characterized continuity between thin/scattered clouds and high turbidity events is another. On the liability side, questions may be raised because (i) model validity should be limited to the domain covered by experimental data, and (ii) the models may carry possible instrumentation limitations (e.g., calibration). Concerning the first point, the validation domain covers a wide climatic/seasonal range, even for the daylight availability models. Further validation/development is, of course, recommended, particularly for drastically different environments—the proposed CIE's International Daylighting Year[41] should provide an excellent basis to address these questions. Concerning the second reservation, the authors believe that, given the care and scrutiny used for instrumentation characterization and cross-calibration, resulting imprecision should be small (this should be of most concern for luminous efficacy models, which are crucially dependent on instrument absolute calibration; in this case it is believed that overall instrumentation-induced model bias should not exceed 3%.

Beyond this first comprehensive set of operational models, further model development yielding enhanced accuracy and/or extended validation is needed and likely to occur in the future as more data becomes available, particularly with respect to skylight angular distribution. Based on their experience, the authors recommend the highest possible care in data and instrumentation quality monitoring if future data are to fulfil this expectation.

Acknowledgments—The work presented in this paper is the result of research efforts sponsored, respectively, by:

1. The Fond National Suisse de la Recherche Scientifique (grant no. 2000-5.314) and the U.S. National Science Foundation (grant no. INT8712462): Research cooperation between the Universities of Geneva, Switzerland, and Albany, NY).
2. The New York State Energy Research and Development Authority (contract no. 724CONDCS85): New York State daylight availability resource assessment program.
3. Sandia National Laboratories (contract no. 56-5434, U.S. Dept. of Energy): Diffuse irradiance model development.
4. The Ernst and Lucie Schmidheiny Foundation, The Societe Academique de Geneve and Geneva's Department of Public Economy: U. of Geneva's Radiation Model Development Program.

The authors are grateful to W. Berkheiser III and K. Webster of the ASRC, the staff of Sandia National Labs, the Florida Solar Energy Center, SUNY Buffalo, Adirondack Community College, Queens College and New York Polytechnic Institute for their assistance in data acquisition and analysis, to A. Zelenka of the Swiss Meteorological Institute for his comments, to Ted Cannon of SERI for his assistance in instrumentation characterization and to J. Wright and T. Guertin who contributed to elements of this research through their Master's theses.

REFERENCES

1. M. R. Fontoynont, *Simulation of complex window components using a photon-tracing simulation program,* ISES Solar World Congress 1987, Paper 8.7.01, Hamburg, FRG (1987).
2. New York State Energy Research and Development Authority (1989): Daylight Availability Resource Assessment Program: Phase IV Preparation of a Climatological Daylight Availability Data Base, NYSERDA 724-CON-BCS-85, NYSERDA, Albany, NY (1989).
3. DOE 2.1c Simulation Program, DOE 2 Engineering Manual, Energy and Environment Division, Building Energy Simulation Group, Lawrence Berkeley Laboratory (LBL), University of California, Berkeley (1985).
4. Commission Internationale de l'Eclairage, Standardization of Luminous Efficacy Distribution on Clear Skies, Pub. no. 222, CIE, Paris, France (1973).
5. P. Moon and D. Spencer, Illumination from a nonuniform sky, *Illuminating Engineering* **37,** 707–726 (1942).
6. Standardization of Luminous Distribution on Clear Skies, CIE Publications No.22, Paris: International Conference on Illumination (1973).
7. K. Matsuura, *Luminance distributions of various reference skies,* CIE Technical Report of TC 3-09 (1987).
8. J. J. Michalsky, J. L. Berndt, and G. J. Schuster, A microprocessor-based rotating shadowband radiometer, *Solar Energy* **36,** 465–470 (1986).
9. J. J. Michalsky, R. Perez, R. Stewart, B. A. LeBaron, and L. Harrison, Design and development of a rotating shadowband radiometer solar radiation/daylight network, *Solar Energy* **41,** 577–581 (1986).
10. R. Perez, R. Seals, A. Zelenka, and P. Ineichen, Climatic evaluation of models that predict hourly direct irradiance from hourly global irradiance—Prospects for performance improvements, *Solar Energy* **44**(2), 99–108 (1989).
11. A. Kasten, A new table and approximate formula for relative optical air mass, *Arch. Meteorol. Geophys. Bioklimatol. Ser. B,* **14,** 206–223 (1966).
12. C. H. Reitan, Surface dew point and water vapor aloft. *J. Appl. Meteor.* **2,** 776–778 (1963).
13. J. Wright, R. Perez, and J. J. Michalsky, Luminous efficacy of direct irradiance: Variations with insolation and moisture conditions, *Solar Energy* **42,** 387–394 (1989).
14. J. F. Orgill and K. G. Hollands, Correlation equation for hourly diffuse radiation on a horizontal surface, *Solar Energy* **19,** 357–359 (1977).
15. A. P. Brunger, The magnitude, variability, and angular characteristics of the shortwave sky radiance at Toronto, *Doctoral Dissertation in Mechanical Engineering,* University of Toronto, Canada (1987).
16. R. Perez, R. Seals, P. Ineichen, R. Stewart, and D. Menicucci, A new simplified version of the Perez diffuse irradiance model for tilted surfaces, *Solar Energy* **39,** 221–231 (1987).
17. R. Perez, R. Stewart, R. Seals, and T. Guertin, Development and validation of the Perez diffuse radiation

model, Sandia National Labs Report no. SAND88/7030, 250 pp, SNLA, Albuquerque, NM (1988).
18. R. Perez, Daylight resource availability. *Phase II Report* (200 pp), New York State Energy Research and Development Authority, Albany, NY (1987).
19. T. Cannon, Personal communication, SERI, Golden, CO (1986).
20. R. Perez, R. Seals, J. Michalsky, W. Berkheiser III, R. Stewart, and K. Webster, Daylight resource availability, Final report (85 pp) (1988).
21. P. J. Littlefair, The luminous efficacy of daylight, *2nd International Daylighting Conference, Long Beach, CA* (1986).
22. G. Gillette and S. Treado, Correlation of solar irradiance and daylight illuminance for building energy analysis. *ASHRAE Transactions* **91**(1A), 180–192 (1985).
23. M. Navvab, M. Karayel, E. Ne'eman, and S. Selkowitz, Analysis of luminous efficacy for daylight calculations, *2nd International Daylighting Conference, Long Beach, CA* (*and ASHRAE transactions*) (in press).
24. P. Ineichen, Mesures d'Ensoleillement a Geneve (6/86-5/87), Groupe de Physique Appliquee, Universite de Geneve, Switzerland (1988).
25. R. Perez, K. Webster, R. Stewart, and J. Barron, Variations of the luminous efficacy of global and diffuse radiation and zenith luminance with weather conditions, *Solar Energy* **38**(1), 33–44 (1987).
26. P. J. Littlefair, Measurement of the luminous efficacy of daylight, *Lighting Research Technology* (in press).
27. P. R. Tregenza, Guide to recommended practice of daylight measurement—General class stations, *Supplement to CIE Journal* **6**(2), (1987).
28. M. Navvab, M. Karayel, E. Ne'eman, and S. Selkowitz, Analysis of atmospheric turbidity for daylight calculations, First International Daylighting Conference, Phoenix, AZ, and *Energy and Building* **6**(3), (1983).
29. S. Aydinli, Uber die Berechnung der zur Verfugung Stehenden Solar-energie und des Tageslichtes, *Doctoral Dissertation,* Tech University of Berlin, Federal Republic of Germany (1981).
30. P. Ineichen, R. Perez, and R. Seals, The importance of correct albedo determination for adequately modeling energy received by tilted surfaces, *Solar Energy* **39,** 221–232 (1987).
31. D. F. Menicucci, J. P. Fernandez, User's manual for PVFORM: A photovoltaic system simulation program for stand-along and grid-interactive applications, Report no. SAND85-0376-UC-276, Sandia National Laboratories, Albuquerque, NM (1988).
32. Daylighting—Lumen method calculation, In: *IES lighting handbook reference volume,* (Ch. 7), Illumination Engineering Society (IES), New York, (1981).
33. R. Perez, R. Stewart, C. Arbogast, R. Seals, and J. Scott, An anisotropic hourly diffuse radiation model for sloping surfaces—Description performance validation, site dependency evaluation, *Solar Energy* **36,** 481–498 (1986).
34. International Energy Agency Solar Heating and Cooling Programme, Task IX B (Validation of Solar Irradiance Simulation Models), IEA, Paris (1987).
35. National Science Foundation International Programs Project no. INT8712462 NSF, Washington, DC. 2.
36. K. Y. Kondratyev, *Radiation in the atmosphere.* Academic Press, New York (1969).
37. J. E. Hay and J. A. Davies, Calculation of the solar radiation incident on an inclined surface, *Proc. First Canadian Solar Radiation Workshop,* Hay & Won, Toronto, Ont., Canada (1980).
38. R. Dogniaux, Variations quantitatives et qualitatives des composantes du rayonnement solaire sur une surface horizontale per ciel serain en fonction du trouble atmospherique, *Pub. IRM-B-62,* Royal Meteorological Institute, Bruxelles, Belgium (1970).
39. M. Karayel, M. Navvab, E. Ne'eman, and S. Selkowitz, Zenith luminance and sky luminance distribution for daylighting calculations, *Energy and Buildings* **6**(3), (1983).
40. M. Perraudeau, Luminance models, National Lighting Conference and Daylighting Colloquium, Robinson College, Cambridge, England (1988).
41. Commission Internationale de l'Eclairage, Announcement by President H. W. Bodmann of International Daylight Measurements Year 1991, managed by TC 3-07 (1987-12-18).
42. P. Ineichen, Mesures de rayonnement a Geneve. Groupe de Physique Appliquee, Universite de Geneve, Geneva, Switzerland (1988).
43. Direction de la Meteorologie, Service Meteorologique Metropolitain, Stations #260 and #874, ONM, Paris (1979–1981).
44. USDOE's Solar Energy Meteorological Research and Training Sites Region II, Atmospheric Sciences Research Center, Albany, NY (1980–1982).
45. New York State Daylight Availability Resource Assessment Program, NYSERDA contract 724-CONBCS85 Atmospheric Sciences Research Center, Albany, NY (1986–1988).
46. Sandia National Laboratories' Measurement Program for Radiation Modeling Contract no. 56-5434, SNLA Albuquerque, NM (1986).

NOMENCLATURE

Z	solar zenith angle (rads., unless otherwise specified)
S	Tilted plane slope angle (rads.)
θ	Solar incidence angle on tilted plane (rads.)
γ	Elevation angle for luminance direction in the sky dome (rads.)
γ_s	Solar elevation angle (rads.)
ζ	Angle between direct beam and considered luminance direction (rads.)
m	Relative optical air mass
W	Atmospheric precipitable water (cm)
T_d	Surface dew point temperature (°C)
G	Global horizontal irradiance (W/m^2)
g	Global horizontal illuminance (Lux)
I	Normal incidence direct irradiance (W/m^2)
I_o	Extraterrestrial normal incidence irradiance (W/m^2)
i	Normal incidence direct illuminance (Lux)
Dh	Horizontal diffuse irradiance (W/m^2)
dh	Horizontal diffuse illuminance (Lux)
Dc	Diffuse irradiance on a tilted plane (W/m^2)
dc	Diffuse illuminance on a tilted plane (Lux)
Xc	Generic term for both diffuse irradiance and illuminance on a tilted plane
Xh	Generic term for both horizontal diffuse irradiance and illuninance
Lvz	Luminance at the sky's zenith (Cd/m^2)
Lvc	Luminance at a given position in the sky (Cd/m^2)
$L'vc$	Normalized luminance at a given position in the sky (Cd/m^2)
G_{eff}	Global luminous efficacy (Lm/W)
D_{eff}	Diffuse luminous efficacy (Lm/W)
I_{eff}	Direct luminous efficacy (Lm/W)
L_{eff}	Zenith luminance "Pseudo-efficacy" Lvz/Dh (Cd/W)
ϵ	Atmospheric clearness parameter (dimensionless)
Δ	Atmospheric brightness parameter (dimensionless)
F_1	Circumsolar brightening coefficient (dimensionless)
F_2	Horizon brightening coefficient (dimensionless)
ψ	Ratio between sky luminance at a given point in the sky and zenith luminance
ψ_{os}	Same as above—CIE overcast sky formulation
ψ_{is}	Same as above—CIE intermediate sky formulation
ψ_{cs}	Same as above—CIE clear sky formulation
ψ_{ts}	Same as above—CIE clear-turbid sky formulation